Propagation law of external fire in excavated tunneling working face in coal mine

Qing GUO [a,*], Wanxing REN [b], Shengcheng WANG [a], Hao WANG [c], Xiaowei ZHU [d], Yuguo WANG [b]

a. School of Civil Engineering, Xuzhou University of Technology, Xuzhou, 221018, China

b. School of Safety Engineering, China University of Mining and Technology, Xuzhou 221116

c. College of Ocean Science and Engineering, Shanghai Maritime University, Shanghai, 200135

d. Jiangsu Dingye Information Technology Co., Ltd. Xuzhou, 221018, China

Corresponding author: GUO Qing, School of Civil Engineering, Xuzhou University of Technology, Xuzhou, 221018, China, E-mail: zgkdgq@163.com

Abstract: To understand the propagation of external fires in excavated tunnels, a combustion model was established using fire dynamics software to analyze the propagation of temperature, airflow, and smoke in excavated tunnels under specific wind speeds and fire source powers. The study shows that smoke propagation can be divided into initial combustion and stable combustion phases, significantly influenced by airflow. In the initial phase, smoke mainly spreads longitudinally. As time progresses, smoke rapidly diffuses to both sides of the tunnel under airflow, forming vortex zones where airflow and smoke converge at tunnel ends. This results in local fluid and thermal circulation, creating localized high-temperature areas. In the stable combustion phase, smoke spreads throughout the tunnel, with significant stratification of airflow at the tunnel end. The enthalpy flow of smoke positively correlates with proximity to the heat source, and the enthalpy difference between adjacent cross-sections at equal distances follows consistent patterns. Grid independence verification was conducted to ensure the accuracy of numerical simulation, and the simulation results were validated by comparison with actual mine fire accident data. This research reveals the fire propagation law under the coupling effect of wind speed and fire source power, providing a scientific basis for improving mine safety management and emergency response capabilities, and offering important theoretical guidance for underground personnel evacuation and rescue.

Key words: Excavated working face; external fire; smoke spread; temperature distribution

1. Introduction

Coal is one of the main energy sources, widely used in the fields of electricity, steel, and chemicals, and still occupies an important position in global energy consumption, especially in China. In 2023, the raw coal production reached 4.71 billion tons, and the proportion of coal in primary energy consumption is close to 60%. Therefore, the safe mining of coal plays an important role in ensuring energy security, stabilizing fuel supply, and building the national economy [1].

Fire is one of the major disasters facing mine production, which can be divided into external and internal causes. Internal fires are mainly caused by coal spontaneous combustion, while external fires are caused by factors such as welding, equipment overheating, and combustible material ignition [2,3]. In recent years, the proportion of cable fires and conveyor belt fires has been gradually increasing, such as the "4.30" cable fire accident in Yujialiang Coal Mine (1 person injured), the "8.1" cable fire accident in Shennan Wulannuoerlun Coal Mine, the "11.19" fire accident in the excavated face of Shandong Liangbaosi Coal Mine, the "9.24" fire accident in Guizhou Shanjiaoshu Coal Mine (16 deaths, 3 injuries), the "9.27" major fire accident in

Chongqing Nengou Songlao Coal Mine (16 deaths, 42 injuries), and the "2.11" fire accident in the ventilation shaft of Mengcun Mine (2 deaths, 7 injuries).

The main characteristics of external fires include the generation of a large amount of smoke, the rise in roadway temperature, the decrease in visibility, and the release of toxic and harmful gases, which not only cause personnel burns and poisoning deaths, but also lead to airflow reversal and damage to the ventilation system. To understand the law of smoke propagation in external fires, domestic and foreign scholars have conducted in-depth research. Wang Xiaodong et al [4] studied the influence of mobile heat sources on the thermal environment parameters in the excavated roadway, pointing out that the mobile heat source in operation is the key factor affecting the macro-temperature field in the roadway. Li Minjie[5] studied the combustion and propagation characteristics of conveyor belt fires in coal mine underground transportation roadways, analyzing the temperature distribution and smoke propagation law of roadway belt fires under different wind speeds, and pointing out that the high-temperature area is mainly distributed in the smoke flow area and maintains a stable thermal stratification state along the entire roadway length. Zhang et al [6] studied the propagation law of L-shaped roadway fires and analyzed the behavior of high-temperature smoke propagation under different wind speeds. Li et al [7] studied the evolution law of full-scale roadway/tunnel fires. HAN [8], Li et al [9] studied the influence of wind speed on the propagation law of mine fires. Tian [10], Wang [11], Qi et al [12] studied the evolution law of mine belt fires and the optimal parameters of the fine water mist extinguishing system. Chen et al [13] established a branched model prediction model for the maximum temperature rise of tunnel roofs under different fire source positions. Liu Yuqing [14], GAO et al [15] studied the propagation law and control technology of smoke in high-slope inclined roadway fires. Jia Jing [16], WANG et al [17] studied the law of smoke flow reversal and critical wind speed changes in mine roadway fires. Tian and other researchers [18-20] based on Pyrosim, studied the influence of wind speed on the propagation law of mine fires, and established a mathematical model of the stable temperature of external mine fires with fire source distance and wind speed. Liu et al [21] used CFD numerical simulation to study the length of the smoke backflow layer in horizontal roadways. Wang et al [22] studied the influence of slope on the flow of smoke in roadway fires, and analyzed the characteristics of temperature, pressure, and smoke propagation in the roadway during the fire.

The above studies have not considered the changes in the development law of fires under the coupled effect of wind speed and fire source. In view of this, this paper uses the FDS fire dynamics simulation software to analyze the propagation process of temperature, airflow, and smoke in the roadway under a certain wind speed and fire source power, and deeply explore the propagation law of external fires in excavated roadways, providing reference for guiding underground personnel evacuation and rescue.

2. Smoke Propagation Control Equations

Tunnel excavated belongs to the underground confined space, and the propagation of smoke inside the tunnel is affected by the structures (obstacles), tunnel dimensions, air flow rate, temperature, etc. The smoke propagation follows the continuity equation, momentum equation, energy equation, and diffusion equation. The Large Eddy Simulation (LES) turbulence model embedded in FDS is adopted for the calculation of turbulent flow in the fire smoke field, which is suitable for simulating the complex turbulent flow characteristics of fire smoke in confined spaces. The specific control equations include:

The continuity equation describes the mass conservation of smoke, as shown in Equation (1):

$$\frac{\partial \rho}{\partial t} + \nabla \cdot (\rho \mathbf{u}) = 0 \quad (1)$$

The gas momentum conservation follows the Navier-Stokes equation, and the momentum conservation equation is shown in Equation (2):

$$\frac{\partial (\rho \mathbf{u})}{\partial t} + \nabla \cdot (\rho \mathbf{u}\mathbf{u}) = -\nabla p + \mu \nabla^2 \mathbf{u} + \mathbf{f} \quad (2)$$

The energy equation is shown in Equation (3):

$$\frac{\partial (\rho e)}{\partial t} + \nabla \cdot (\mathbf{u}(\rho e + p)) = \nabla \cdot (k \nabla T) + Q \quad (3)$$

Furthermore, the change in smoke concentration follows the diffusion equation, as shown in Equation (4):

$$\frac{\partial C}{\partial t} = D \nabla^2 C \quad (4)$$

Where: ρ is the smoke density, kg/m³; u is the velocity field, m/s; t is the time, s; ∇ is the Hamilton operator; p is the pressure, Pa; μ is the dynamic viscosity, Pa·s; f is the body force, N/m³; e is the internal energy, J; k is the thermal conductivity, W/(m·K); T is the temperature, K; Q is the heat source, J/s; C is the smoke concentration, kg/m³ ; D is the diffusion coefficient, m² /s.

The fire smoke flow process is mainly affected by its own buoyancy, gravity, viscous force, and inertial force, and the heat transfer in the combustion process mainly involves convection, conduction, and radiation. As the smoke propagates and the heat diffuses, the tunnel temperature rises, the internal energy increases, and the gas expands due to heating, leading to an increase in the enthalpy flow rate of the smoke. The enthalpy calculation formula is shown in Equation (5):

$$H = e + pV \quad (5)$$

When the pressure change in the tunnel is relatively small, the combustion process is considered an isobaric process, and the heat capacity is the isobaric heat capacity C_p. The enthalpy difference calculation formula for the combustion process is:

$$\Delta H = \int_{T_1}^{T_2} C_p(p, T) dT = C_p (T_2 - T_1) \quad (6)$$

That is, the enthalpy difference of the smoke in the tunnel is positively correlated with the temperature difference.

Where: C_p is the isobaric heat capacity, J/(kg·K); V is the smoke volume, m³ .

3. Numerical Calculation Model

3.1 Fire Model in Excavated Roadway

An excavated roadway model is constructed using an external fire incident during positive pressure ventilation in a developing roadway as an example, and the geometrical and working parameters of the model are determined based on the actual layout of coal mine excavated working faces in China and the Code for Ventilation Design of Coal Mines (GB 50215-2015). The roadway's geometric parameters are length × width × height = 300 m×4 m×5 m, as shown in Figure 1. The origin of the coordinate system is marked as O(0, 0, 0). The ventilation duct is located 5 m from the excavated face, with a cross-sectional size of 0.8 m × 0.8 m. The positive pressure ventilation airflow rate is 600 m³/min, with a leakage rate of 5% (the average leakage rate of mine ventilation ducts in actual engineering).

Boundary conditions of the model are set as follows: the roadway wall is set as an adiabatic

solid boundary (consistent with the thermal insulation characteristics of mine rock mass); the ventilation duct outlet is set as a velocity inlet boundary to simulate the forced air supply of the local fan; the roadway end is set as a pressure outlet boundary to simulate the air exchange with the external space of the roadway.

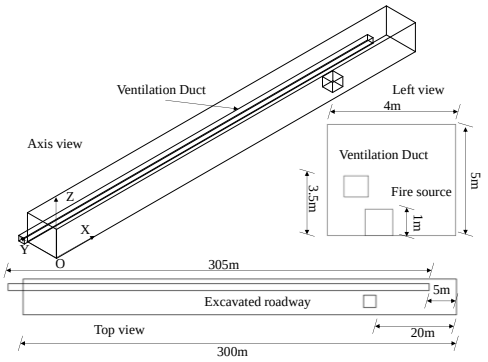

Figure 1 Model geometric parameters

The model incorporates coal, pine wood, and polyurethane as materials. The model includes nine temperature detectors and four smoke concentration detectors. The coordinates of the temperature detectors are (140, 2.0, 1.8), (160, 2.0, 1.8), (170, 2.0, 1.8), (175, 2.0, 1.8), (180, 2.0, 1.8), (190, 2.0, 1.8), (200, 2.0, 1.8), (270, 2.0, 1.8), and (295, 2.0, 1.8). The smoke concentration detectors are located at cross-sections X = 140 m, 160 m, 180 m, and 200 m. To more effectively observe the spread of smoke and temperature over time, several temperature slices and velocity slices are included in the model.

3.2 Mesh Generation and Fire Source Setting

3.2.1 Mesh Generation and Grid Independence Verification

The rationality of mesh division directly affects the accuracy and calculation efficiency of numerical simulation. In this study, the mesh is encrypted in the fire source and smoke propagation key areas to ensure the simulation accuracy of the high-temperature and high-velocity flow field near the fire source, and the non-key areas adopt regular mesh division to balance the calculation accuracy and efficiency. The final adopted mesh size of the excavated roadway model is 0.2m×0.15m×0.15m, comprising a total of 1,842,750 cells.

Grid independence verification was conducted with three sets of mesh sizes to determine the optimal mesh resolution:0.4m×0.3m×0.3m, total cells: 229,500; 0.2m×0.15m×0.15m, total cells: 1,842,750; 0.1m×0.075m×0.075m, total cells: 14,742,000.

The verification results show that the simulation results of the medium grid (temperature, airflow velocity, smoke propagation distance) are consistent with those of the fine grid (the relative error is less than 5%), while the calculation time of the medium grid is only 1/6 of that of the fine grid. The simulation results of the coarse grid have a large deviation (the relative error is more than 15%) due to the low resolution. Therefore, the medium grid is selected for the final numerical simulation to ensure the simulation accuracy and calculation efficiency.

3.2.2 Fire Source Setting

The fire source setting is based on the statistical characteristics of actual mine external fire accidents (cable and conveyor belt fires are the main types of external fires, and their fire growth rate is between medium and fast fires). The fire source was centrally located 20m from the excavated face, with a burning area of $1m^2$ and a burning surface height of 1m, approximating the height of the conveyor belt (the main fire source position of mine external fires). The reaction type

was set as polyurethane combustion (the main combustible material of mine conveyor belts and cables).

The mine fire development process was modeled using the t^2 fire model, with the heat release rate (HRR) calculated using the following formula[9]:

$$Q=\alpha t^2 \tag{7}$$

where: Q is the heat release rate, kW; α is the fire growth coefficient, kW/s².

The t_2 model categorizes combustion into four standard fire types: slow, medium, fast, and ultra-fast fires. Studies indicate that externally caused mine fires fall between medium and fast fires. This study sets the fire as a fast fire, with α=0.05 kW/s² and a unit area heat release rate (HRR) of 5 MW/m². The numerical simulation time was set to 1000s, with an ambient temperature of 20℃. The simulation investigated the propagation patterns of smoke and temperature in the excavated roadway under single-heat-source conditions.

4. Analysis of Fire Spread Patterns in a Mining Face

4.1 Characteristics of Airflow Distribution

The maximum airflow velocity in the excavated tunnel occurs at the outlet of the local ventilation fan. The airflow initially impacts the area between the fan outlet and the mining face, causing backflow and the formation of vortices. The strongest vortices are located in the area where the mining face wall meets the tunnel sidewall, away from the local ventilation fan (Figure 2). Fire spread significantly affects airflow distribution. Six seconds before the fire incident, the mechanical airflow and the airflow induced by smoke spread are independent. After 8 seconds, the two airflow patterns converge (Figures 3 and 4). The smoke from the fire is primarily distributed in the upper part of the tunnel, while the mechanical airflow is distributed in the lower part. After the airflow converges, a new vortex region forms, approximately 14m in length, centered about 1.7m below the tunnel ceiling. The location of this vortex region remains relatively stable.

In the later stages of combustion, the airflow distribution downwind of the ignition point stabilizes, with velocity decreasing from the top to the bottom of the tunnel, exhibiting distinct velocity zones. This airflow stratification phenomenon is the result of the coupling of smoke buoyancy and mechanical ventilation airflow: the smoke heated by the fire source has a lower density and rises to the roadway ceiling, forming a high-velocity smoke flow layer under the action of mechanical ventilation; the lower part of the roadway is a low-velocity cold air layer with higher density, and the two layers form a clear interface due to the density difference. In addition, the local vortex zone formed by the convergence of thermal airflow and mechanical airflow restricts the vertical mixing of airflow, which further enhances the stratification phenomenon.

As the fire spreads, the high-velocity region gradually moves downward, stabilizing after 160 seconds, resulting in a stable smoke layer height (Figure 5), because the heat release rate of the fire source and the smoke buoyancy reach a dynamic balance with the mechanical ventilation, resulting in a stable smoke layer height.

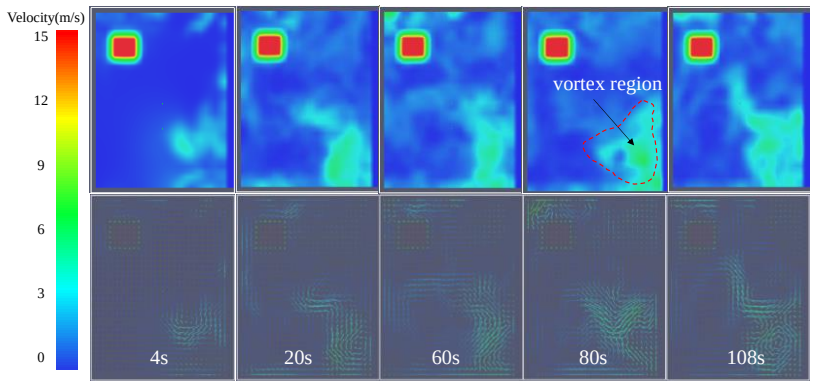

Figure 2 Airflow velocity distribution of air duct outlet（X=295m）

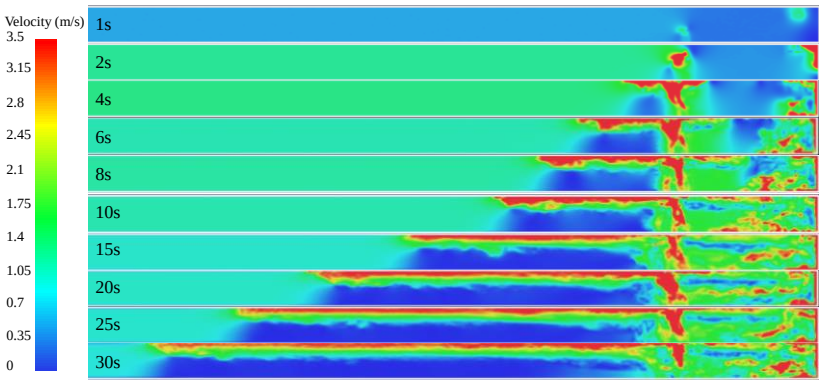

Figure 3 Cloud map of wind speed distribution in tunnel cross-section（Y=2m）

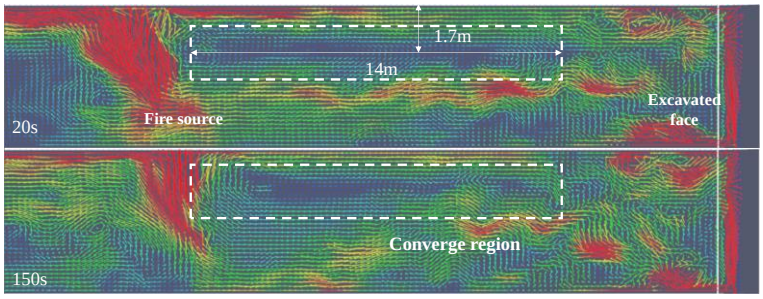

Figure 4 Flue gas intersects with mechanical airflow

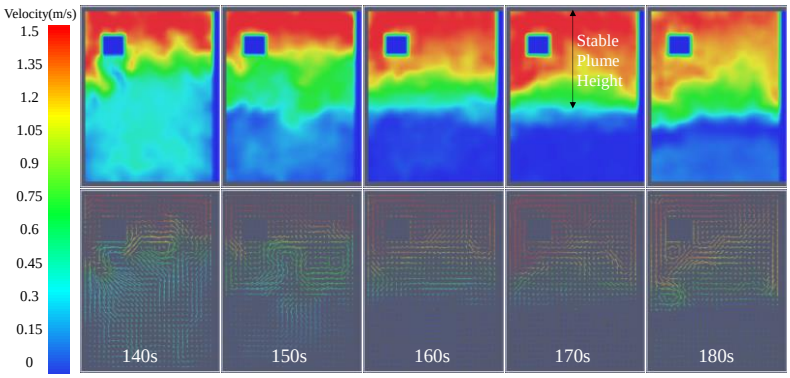

Figure 5 Wind speed distribution at the end of the tunnel（X=5m）

4.2 Smoke Propagation Pattern

Smoke propagation is primarily influenced by airflow. The entire smoke propagation process

can be divided into two stages: the initial combustion stage and the stable combustion stage, and the smoke propagation characteristics in the two stages are significantly different under the coupling effect of wind speed and fire source power.

In the initial stage of combustion, smoke spreads longitudinally, as shown in Figure 6. At 1 second, the smoke spreads outward from the burning material. Then, under the influence of airflow, the smoke spreads to the right side and top of the roadway along the airflow. At 14 seconds, it fills the roadway's cross-section. During this stage, the smoke area's ratio to the roadway cross -section is 14.5% (1s), 36.7% (2s), 65.5% (4s), 70.8% (8s), 72.2% (10s), and 100% (14s), respectively. Based on the smoke area ratio, the initial smoke propagation can be divided into three stages: before the convergence of the mechanical airflow and the combustion airflow, the smoke propagation is divided into rapid and stable stages; after the convergence of the two airflows, the smoke propagation becomes rapid.

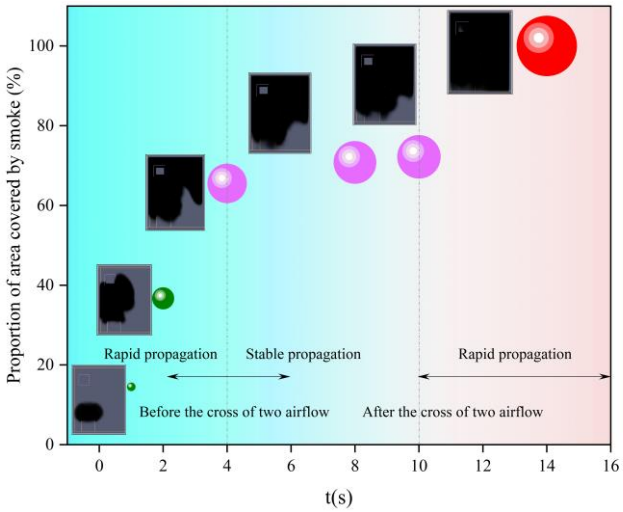

Figure 6 Longitudinal distribution of smoke height at the heading face of excavated roadway

In the initial combustion phase, smoke is distributed around the fire source. During the stable combustion phase, the smoke reaches the roadway ceiling and rapidly spreads laterally. Under the influence of local ventilation, some smoke spreads rapidly towards the outlet along the airflow, while the other part spreads towards the heading face. The smoke reached the heading face at 12 seconds, covered the longitudinal cross-section of the roadway at 14 seconds, and recirculated to the fire source from the right side at 18 seconds. Thereafter, the smoke spread steadily, filling the entire roadway in approximately 250 seconds (Figure 7). Influenced by the airflow, the initial smoke spread rate differed on either side of the fire source, resulting in a disparity in the spread distance. The ratio of smoke spread distance to the left versus the right of the fire source was approximately 1.7 (Figures 8 and 9).

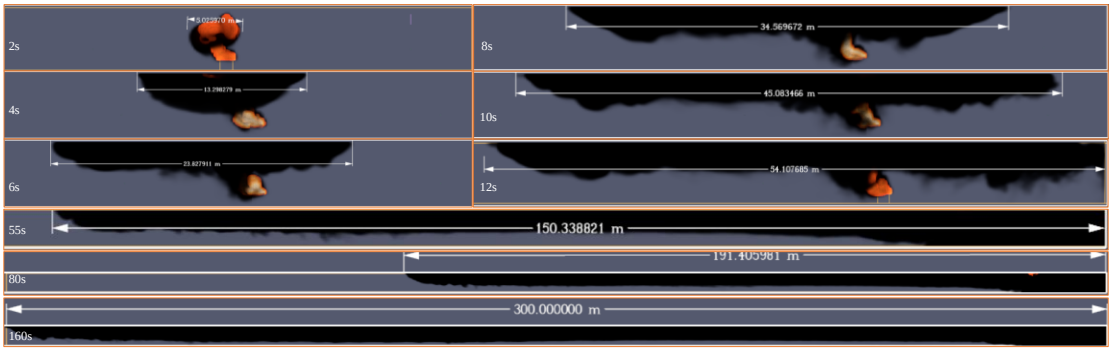

Figure 7 Smoke spreads and distributes along the direction of the tunnel

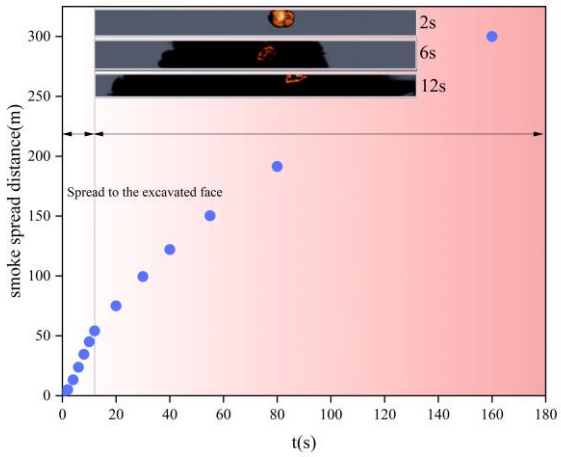

Figure 8 Length of smoke propagation along the tunnel

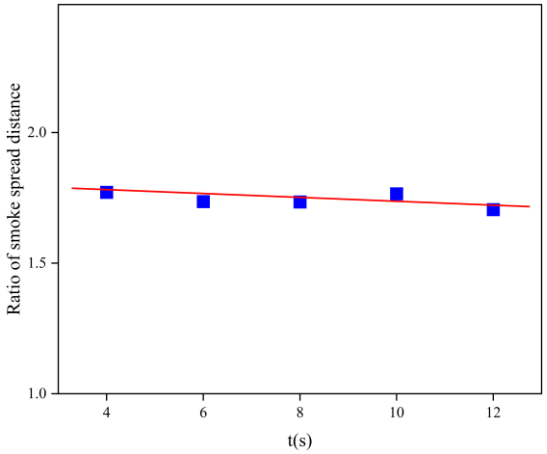

Figure 9 Ratio of smoke spread distance to the left side versus the right side

4.3 Temperature Propagation Pattern

The temperature distribution within the roadway is primarily influenced by the spread of smoke. Figure 10 shows the temperature distribution cloud chart at Z =1.8 m. This indicates that the highest temperature of the smoke in the roadway is approximately 70℃. In the initial stage of combustion, the highest temperature is near the burning material. After the mechanical airflow and hot airflow converge (after 12 s), the high-temperature zone is mainly distributed in the airflow convergence zone, i.e., between the heat source and the end of the development roadway. The main reason for this phenomenon is that the smoke in the airflow convergence zone is in a vortex state, forming a local circulating airflow, and heat accumulation causes the temperature to rise. The temperature on the leeward side of the burning material gradually decreases. The temperature near the roadway walls is slightly higher than that in the middle because smoke accumulates at the walls, carrying more heat, thus resulting in higher temperatures.

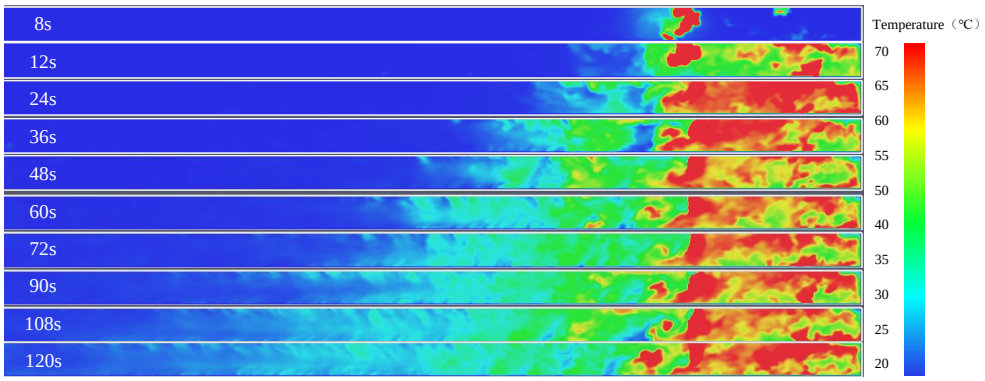

Figure 10 Distribution of temperature (Z=1.8m）

Figure 11 shows the temperature changes at each measuring point during the entire combustion process. Measuring points 1 and 9 are located on the leeward and windward sides of the fire source, respectively, at distances of 30 m (15 m) and 5 m (10 m) from the development heading (or heat source). The times required for the temperatures at these two points to reach equilibrium are 30 s and 50 s, respectively. After equilibrium, the highest temperature at measuring point 1 is 71℃, and the average temperature is approximately 60℃; the highest temperature at measuring point 9 is 55℃, and the average temperature is 45℃. Other measuring points are located sequentially on the leeward side of the fire source. After 25 s, the temperature begins to rise. When the smoke spreads to the entire roadway, the highest temperature at the measuring points is 33℃, and the temperature difference between adjacent measuring points is small. After 200 s, the temperature at each measuring point is basically stable.

Model validation was conducted by comparing the simulation results with actual mine fire accident data: the highest temperature in the "11.19" fire accident at Shandong Liangbaosi Coal Mine[23] was 78℃, and the highest temperature in this simulation is 71℃, with a difference of only 7℃ (the relative error is 9%), indicating that this simulation conforms to the actual conditions of mine external fires and has high reliability. In addition, the model's basic control equations and fire source setting are consistent with the verified mine fire simulation models in existing high-quality literature (e.g., Tian et al., 2020; Li et al., 2022), further verifying the rationality of the model.

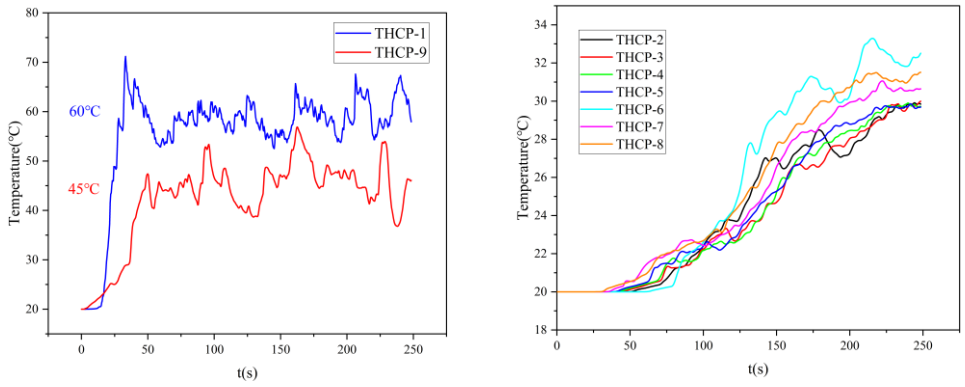

Figure 11 Temperature variation curves at different measurement points in the excavated tunnel

Figure 12 shows the enthalpy change across different cross-sections. The closer to the heat source, the greater the enthalpy of the flue gas, which is due to the gradual heat loss of smoke during propagation: the smoke near the heat source has a high temperature and internal energy,

and the enthalpy flow is large; as the smoke propagates away from the heat source, heat is transferred to the roadway wall through convection and radiation, the smoke temperature decreases, the internal energy and volume shrink, and the enthalpy flow decreases accordingly. Figure 13 shows the enthalpy difference between adjacent cross-sections. The flue gas reached four cross-sections at 55s, 66s, 79s, and 92s respectively. The enthalpy difference fluctuated stably. Based on the temperature change characteristics at each measurement point, during the stable combustion phase, the temperature gradient on the leeward side of the heat source did not change significantly, meaning the temperature difference changed smoothly. According to equation (6), the enthalpy difference between adjacent cross-sections showed relatively small fluctuations. The stable enthalpy difference between adjacent cross-sections at equal distances is the embodiment of the stable heat loss rate of smoke in the uniform roadway section: the roadway has the same cross-section size and thermal conductivity, so the smoke heat loss per unit distance is basically the same, which conforms to the energy conservation law in the process of smoke advection and heat transfer.

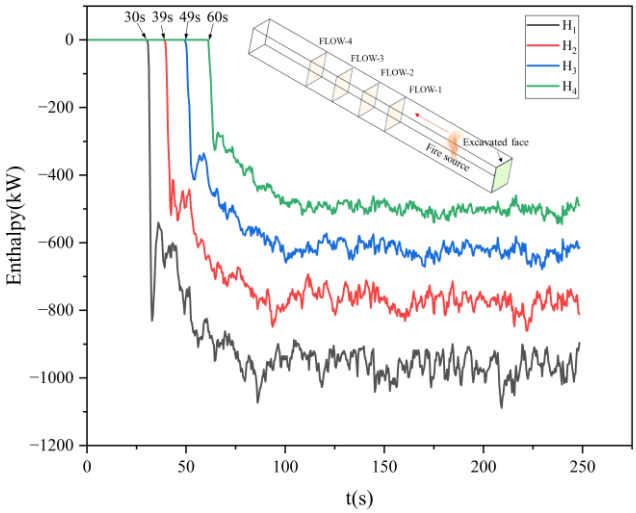

Figure 12 Enthalpy flow curves for different cross-sections over time

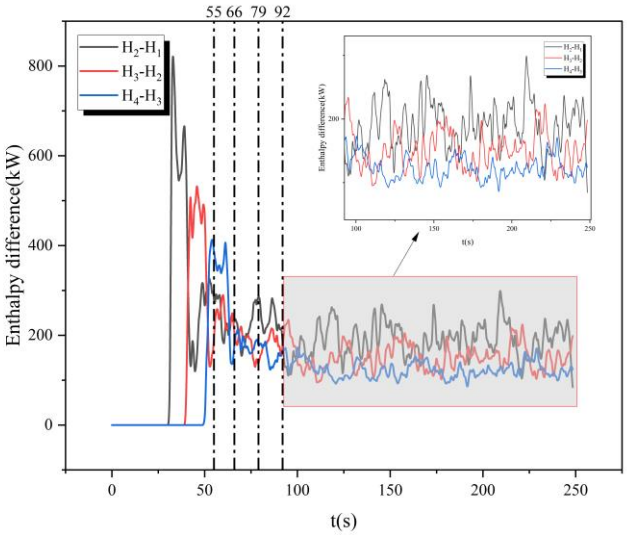

Figure 13 Enthalpy difference curve over time

5. Conclusion

This paper established a model for the propagation of fires in excavated roadways under

single heat source and fixed wind speed conditions based on the actual engineering parameters of coal mines, adopted FDS software for numerical simulation with grid independence verification and model validation by actual accident data, analyzed the patterns of airflow, temperature, and smoke propagation under the coupling effect of wind speed and fire source power, and pointed out that combustion can be divided into an initial stage and a stable stage, with different fire propagation characteristics in the two stages. The main conclusions are as follows:

（1）In the initial combustion stage, the smoke rises under the influence of heat and then propagates to both sides of the fire source after reaching the roof of the roadway, with the downwind propagation speed being about 1.7 times the upwind propagation speed; the smoke fills the entire cross-section of the roadway at 14 s, and the initial smoke propagation can be divided into three stages according to the smoke area ratio: rapid propagation, stable propagation, and secondary rapid propagation, which is closely related to the convergence of mechanical airflow and combustion airflow. In the late stage of stable combustion, there is a significant stratification phenomenon in the airflow, with the flow velocity gradually decreasing from top to bottom. This phenomenon is the result of the coupling of smoke buoyancy and mechanical ventilation airflow, and the local vortex zone further enhances the airflow stratification; the airflow stratification stabilizes after 160 s, forming a stable smoke layer height.

（2）The thermal airflow caused by combustion and the mechanical ventilation airflow converge on the upwind side of the fire source, forming a local vortex area with a length of about 14 m, which exists throughout the combustion stage and leads to the accumulation of heat, forming a high-temperature region (the maximum temperature is about 71℃); the temperature near the roadway walls is slightly higher than that in the middle due to smoke accumulation.

（3）The smoke enthalpy flow is positively correlated with the proximity to the heat source due to the gradual heat loss of smoke during propagation; the enthalpy difference between adjacent cross-sections at equal distances remains stable in the stable combustion phase, which is the embodiment of the stable heat loss rate of smoke in the uniform roadway section and conforms to the energy conservation law.

Acknowledgement

The work was supported by National Natural Science Foundation of China (NO:52404230).

Nomenclature

ρ is the smoke density, kg/m³;
u is the velocity field, m/s;
t is the time, s;
∇ is the Hamilton operator;
p is the pressure, Pa;
μ is the dynamic viscosity, Pa·s;
f is the body force, N/m³;
e is the internal energy, J;
k is the thermal conductivity, W/(m·K);
T is the temperature, K;
Q is the heat source, J/s;
C is the smoke concentration, kg/m³ ;

D is the diffusion coefficient, m^2 /s;
C_p is the isobaric heat capacity, J/(kg·K);
V is the smoke volume, m^3 ;
Q is the heat release rate, kW;
α is the fire growth coefficient, kW/s^2.

References

[1] Xie, H.P., Ren, S.H., Xie, Y.C., et al., Development of Electricity Generated from Zero-Carbon Clean Coal: Feasibility and Competitiveness of “Clean Coal Power + CCUS”. Strategic Study of CAE.,26 (2024),4,pp.176-185.

[2] Guo, Q., Ren, W.X., Lu, W., et al., Spontaneous combustion gas evolution law and dangerous zone division of coal in stope face. Journal of China coal Society.,48(2023),S2,pp,647-656.

[3] Zhou, F.B., Xin, H.H., Wei, L.J., et al. Research progress of mine intelligent ventilation theory and technology[J]. Coal Science and Technology.,51(2023),1,pp,313−328.

[4] Wang, X.D., Zhang, Y., Liu, J., et al., Study on the influence of mobile heat source on the thermal environment parameters of roadway. Coal Science and Technology.,52(2025),S2,pp,88-100.

[5] Li, M.J., Study on Belt Combustion and Spread Characteristics of Coal Mine Underground Transportation Lane, Master. thesis, Henan Polytechnic University, Jiaozuo, 2023.

[6] Zhang, C.H., Kang, X., Shen, J.H., Simulation study on fire spread law of L-shaped roadway in mine. Journal of Safety and Environment.,22(2022),6,pp.3111-3118.

[7] LI, Q., Kang, J.H., Zhou, F.B., et al., Prediction model and verification of smoke flow temperature in full-scale roadway/tunnel fires. Journal of Safety Science and Technology.,18(2022),8,pp.5-12.

[8] Han, J.Q., Wang, Fei., Jennifer W., et al. Investigation on the characteristics of fire burning and smoke spreading in longitudinal-ventilated tunnels with blockages. Tunnelling and Underground Space Technology incorporating Trenchless Technology Research,2023,pp.104790.

[9] Li, H., Tian, L., Zeng, G., et al., Study on influence of wind speed on spread law of mine fire based on FDS. Journal of Safety Science and Technology.,18(2022)5,pp.143-149.

[10] Tian, L., Research on the evolution law of mine belt fire and the prevention and extinguishing technology of fine water mist, Master. thesis, Hunan University of Science and Technology, Xiangtan, 2022.

[11] Wang, Y.F., Jiang, J.C., Gong, Y.F., et al. Test research of full-scale tunnel fire and theoretical prediction on the distance of smoke regressing. China Safety Science Journal.,17(2007)8,pp.37-41.

[12] Qi, Q.J., Wang, H., Dong, Z.W., et al., Numerical simulation of belt conveyor fi re spreading law in coal mine. China Safety Science Journal.,26(2016)10,pp.36-41.

[13] Chen, C.K., Jiao, W.B., Lei, P., et al., Numerical simulation analysis on influence of fire source position on critical wind velocity of bifurcated tunnel fire. Journal of Safety Science and Technology.,18(2022),3,pp.93-99.

[14] Liu, Y.Q., Zhang, P.H., Study on fire-induced smoke temperature distribution characteristics in largely inclined roadway. China Safety Science Journal.,31(2021),4,pp.156-162.

[15] Gao, Z., Liu, M., Zhao, P., et al. Influence of tunnel slope on the one-dimensional spread of smoke transportation and temperature distribution in tunnel fires. Tunnelling and Underground Space Technology incorporating Trenchless Technology Research,2024,146105650.

[16] Jia, J., Guo, L.W., Zhu, L.Q., et al., Study on numerical simulation of smoke backflow and critical wind speed in mine roadway fire. Journal of Safety Science and Technology.,16(2020),4,pp.94-100.

[17] Wang, B., Peng, W., Zhong, W., et al. Investigation on smoke propagation behavior and smoke back-layering

length of fires in an inclined tunnel under natural ventilation. Tunnelling and Underground Space Technology incorporating Trenchless Technology Research,2024,150105823.

[18] Tian, S.C., Dou, P.Q., Zhang, C.Z., Impact of different wind speeds on the law of mine fire spread based on pyrosim. METAL MINE.,2(2020),pp.199-204.

[19] Li, Y.F, Wang, H.Y., Zhao, M.X., et al. Fire temperature distribute of sloping tunnels. Fire Science and Technology.,35(2016),12,pp.1677-1679.

[20] Zhang, X.H., Ding, F., Zhang, Y.T., et al. Numerical simulation of underground flue in roadway fire. Safety in Coal Mines., 48(2017),4,pp.48-51.

[21] Liu, J.W., Li, Y.F., CFD numerical simulation of the length of countercurrent layer in level tunnel. Journal of Liaoning Technical University (Natural Science).,33(2014) ,8,pp.1053-1057.

[22] Wang, S.Y., Li, Z.X., Li, J., Slope effects on tunnel fire with numerical simulation. Journal of Liaoning Technical University(Natural Science).,32(2013),12,pp.1590-1594.

[23] Public network.36 Hours of Life Rescue - Liangbaosi Coal Mine "11·19" Accident Rescue Panorama Record. https://baijiahao.baidu.com/s?id=1656471959042515644&wfr=spider&for=pc. 2020.01.23.

Submitted: 5.12.2025.
Revised: 19.3.2026.
Accepted: 23.3.2026.